China Geology 8 (2025) 26–38

China Geology

Journal homepage: http://chinageology.cgs.cn
https://www.sciencedirect.com/journal/china-geology

Optimization of lithium extraction solar pond in Zabuye Salt Lake: Theoretical calculation combined with field experiments

Tao Ding[a], Zhen Nie[a,*], Qian Wu[a], Jiang-jiang Yu[a], Ling-zhong Bu[a], Yun-sheng Wang[a], En-yuan Xing[a], Mian-ping Zheng[a], Yu-bin Li[b]

[a] *MNR Key Laboratory of Saline Lake Resources and Environments*, *Institute of Mineral Resources*, *Chinese Academy of Geological Sciences*, *Beijing* 100037, *China*
[b] *College of Engineering*, *Tibet University*, *Lhasa* 850000, *China*

ARTICLE INFO

Article history:
Received 11 May 2024
Received in revised form 9 August 2024
Accepted 15 August 2024
Available online 31 October 2024

Keywords:
Salt lake
Solar pond
Lithium extraction
Crystallization rate
Box-Behnken
Computational fluid dynamics
Response surface
Zabuye salt lake
Mineral exploration engineering

ABSTRACT

This research optimized the structure of lithium extraction solar ponds to enhance the crystallization rate and yield of Li_2CO_3. Using the response surface methodology in Design-Expert 10.0.3, the authors conducted experiments to investigate the influence of four factors related to solar pond structure on the crystallization of Li_2CO_3 and their pairwise interactions. Computational Fluid Dynamics (CFD) simulations of the flow field within the solar pond were performed using COMSOL Multiphysics software to compare temperature distributions before and after optimization. The results indicate that the optimal structure for lithium extraction from the Zabuye Salt Lake solar ponds includes UCZ (Upper Convective Zone) thickness of 53.63 cm, an LCZ (Lower Convective Zone) direct heating temperature of 57.39°C, a CO_3^{2-} concentration of 32.21 g/L, and an added soda ash concentration of 6.52 g/L. Following this optimized pathway, the Li_2CO_3 precipitation increased by 7.34% compared to the initial solar pond process, with a 33.33% improvement in lithium carbonate crystallization rate. This study demonstrates the feasibility of optimizing lithium extraction solar pond structures, offering a new approach for constructing such ponds in salt lakes. It provides valuable guidance for the efficient extraction of lithium resources from carbonate-type salt lake brines.

1. Introduction

Lithium has the characteristics of high storage energy density and low self-discharge rate. It is used as a cathode material for lithium batteries, which are extensively used in new energy vehicles and portable electronic products in recent years (Wang J et al., 2024). With the concern of environmental factors, such as global climate warming and carbon cycle, the new energy industry based on lithium batteries will further develop in near future. Consequently, the demand for lithium resources will continue to increase (Rioyo J et al., 2022). It was proved that 60% of the world's lithium resources exist in the salt lake brine (Ding T et al., 2023), which makes it of great economic and environmental significance to efficiently extract lithium resources from the salt lake brine.

The current processes for extracting lithium from salt lake mainly include adsorption+membrane (Ding T et al., 2022), extraction+membrane (Nie Z et al., 2022) and solar cell (Zheng M et al., 2023). In China, the Tibet region has the largest distribution of lithium-containing salt lakes. Due to its high altitude, fragile ecological environment, large differences in the chemical properties of the salt lake water, scarcity of electric power resources and high cost of energy, the process for extracting lithium from there should be adaptable to the local conditions (Ding T et al., 2022). In a solar pond, the solar energy is used as the energy required by the evaporation crystallization process for extracting lithium, which is simple to operate and no chemical reagent is needed in aspect of the entire process, making it a green production process suitable for lithium extraction in plateau salt lakes (Zheng M et al., 2023). The solar pond is a green energy storage technology that collects solar energy for storing its heat. The structure of the traditional heat storage solar pond is divided into three

First author: *E-mail address*: dtcumtb@163.com (Tao Ding).

* Corresponding author: *E-mail address*: nieezhen518@163.com (Zhen Nie).

Literary editor: Li-qiong Jia
doi:10.31035/cg2024085
2096-5192/© 2025 China Geology Editorial Office.

layers from top to bottom, which are Upper Convective Zone (UCZ), Non-Convective Zone (NCZ) and Lower Convective Zone (LCZ). In the UCZ layer, usually fresh water is used, while some experiments use depleted brine also. Its temperature is close to the ambient temperature, and it is greatly influenced by the surrounding environment. For storing heat and generating power, its thickness is generally set to 0.2–0.9 m. The NCZ layer is a structure with a gradient distribution of salt concentration, whose thickness is generally set to 1–1.5 m. In this layer, the salinity and temperature increase with increasing depth. It is an anti-convection layer, which is the basis for ensuring a stable operation of the solar pond. The LCZ layer is composed of high-concentration brine, which is the heat storage layer of the solar pond with temperature reaching up to 60–95°C (Nie Z et al., 2011; Kaushika ND, 1984). The study on the application and extraction of heat energy from the salt gradient of a solar pond is a research hotspot. The factors that influence its heat storing performance include salt working medium, turbidity of brine, structure, temperature, and climatic conditions, among others (Bozkurt I et al., 2015; Alcaraz A et al., 2018). The salt working medium is the main heat carrier in the brine. Usually sodium chloride, magnesium chloride and magnesium sulfate are used to configure the brine in different proportions. The past findings indicated that the larger the molecular weight of the salt working medium in the NCZ layer brine, the higher the solubility, the more stable the layer, and the better the performance of the heat storage. If the specific heat capacity of the salt working medium is small, the NCZ layer heats up faster. In the study of the influence of the structure of the solar pond on its heat storing performance, scientists focused on the cover, thickness and shape of the insulation of the NCZ layer. In order to address the influencing factors of a solar pond on its heat storage, researchers proposed to add porous media materials, phase transition materials and nano-adsorbed particles to the salt water for improving its heat storage performance. Addition of porous media materials (including silicon carbide foam ceramics, coal cinder and different soils) is considered mainly to achieve low density, large specific surface area and good heat storage performance (Sayer AH et al., 2018; Bisht S et al., 2020).

The phase transition materials are mostly selected from paraffin wax having high latent heat of fusion and less pollution. These materials are used for enhancing the heat storage stability of salinity-gradient solar ponds. Addition of phase transition materials could reduce the maximum temperature differences in the solar pond during day time and night time by 2.87°C and 2.53°C, respectively. Phase transition materials can enhance the heat storage stability of salinity-gradient solar pond.The addition of nano-adsorbed particles, such as silica gel, iron oxide and zinc oxide, can increase the temperature of the LCZ layer to a certain extent. This research direction needs to be further focused in future (Abdullah AA et al., 2017; Alcaraz A et al., 2018; Li N et al., 2021).

For all we know, the authors were the first to extract lithium from solar pond of salt lakes for industrial application (Zheng MP et al., 2023). For extracting lithium from a solar pond, the original brine was first subjected to multi-stage pre-sunning and high concentration. The brine was completed after Li^+ reached a certain concentration. The prepared brine was then poured into the LCZ layer of the solar pond, and the lithium was extracted using the thermal precipitation properties of lithium carbonate. Tang LJ et al. (2009) conducted a lithium carbonate crystallization test during the process of lithium extraction from carbonate-type salt lakes using an indoor heating solar pond. It was found that the evaporation in the test increased with increasing temperature, but it exhibited minimal effect. The similarities and differences between the lithium extracted experimentally from the solar pond and that simulated at 50°C were analyzed through a comparative study. It was found that temperature played an important role in the lithium extraction. The stable salt gradient could effectively prevent the loss of heat from the LCZ layer, and delay the precipitation of NaCl by diluting the ion concentration (Yu JJ et al., 2013). Based on the heterogeneous nucleation theory, an enhanced solar pond with nucleation matrix was proposed to assist the crystallization of lithium carbonate. Wu Q et al. (2022) Variation in the crystallization behavior of lithium carbonate, and the influences of the matrix material and spatial distribution on the crystallization effect were investigated. The obtained results showed that the enhanced solar pond with a nucleation matrix had a significant effect on the improvement of the lithium carbonate production, and the mixed lithium salt attached to the nucleation matrix had a higher grade and lower water content. However, the current research is focused on the *on-site* process and lithium carbonate crystallization, with a few studies focusing on the mechanism of the structure and distribution of temperature in the solar pond, which leads to a long production cycle and low efficiency in lithium extraction from solar pond. There are few studies on the transmission mechanism of temperature within and between the layers of the solar pond during the crystallization process of lithium carbonate, which is a severe technical bottleneck that needs to be solved urgently.

Based on above, in this study a small solar pond, combined with the Box-Behnken model used in the response surface method, was established for extracting lithium. The structure of the solar pond was optimized by the crystallization effect of lithium carbonate. The flow field inside the solar pond was simulated by the CFD module of the COMSOL Multiphysics software. At the same time, the fluid heat transfer physical field was used in the heat transfer module. In this simulation, the interaction between the flow field and fluid heat transfer is considered to reveal the temperature distribution mechanism in the solar pond, so as to improve its efficiency, stability and life.

2. Experiment

2.1. Solar pond construction

The solar pond was constructed by directly leveling and

excavating earth on the beach of the Zabuye salt lake according to the prescribed design specifications (4 m long, 3 m wide, and 3 m deep), and then laying a liner comprising 8 cm thick concrete and 0.8 mm thick EPDM waterproofing membrane. Then, the solar pond was formed as follows. Firstly, the LCZ layer was formed by filling the solar pond up to a certain depth with brine nearly saturated with lithium carbonate. This is equivalent to the processing container for purifying lithium carbonate by hydrometallurgy. Then, the solar pond was filled with fresh water above the flat surface of the brine for forming a gradient layer by the natural diffusion of the salt. In order to reduce any error in the experiment, fresh water was supplemented regularly to make up for evaporation. The dust and leaves fallen on the surface of the solar pond ware removed periodically for reducing the turbidity of the water and maintaining the homogeneity of the experimental conditions (Fig. 1).

2.2. Data monitoring and sampling

A thermocouple was used to collect the real-time temperature of each layer in the solar pond, and an automatic tracking solar radiometer was used to collect the radiation data synchronously as follows (Tahat MA et al., 2000):

The heat collection Q_c can be expressed by Eq. (1).

$$Q_c = C_L m_L (T_{t+\Delta t} - T_t) \tag{1}$$

where, C_L is the specific heat capacity of the LCZ solution, m_L is the total mass of the LCZ solution, and $T_{t+\Delta t}$ and T_t are the solar pond temperature of the LCZ solution at time t and after the current time interval, respectively.

The heat storage Q_S can be obtained as in Eq. (2).

$$Q_S = C_L m_L (T_{t+\Delta t} - T_0) \tag{2}$$

where, T_0 is the initial temperature of the LCZ solution; T_t is the temperature at time t; and η is the thermal efficiency of the solar pond that can be expressed by Eq. (3).

$$\eta = (C_L \times m_L \times (T_{t+\Delta t} - T_t)) / (((I_{t+\Delta t} + I_t)/2) \times \Delta t \times A_L) \tag{3}$$

where, I_t and $I_{t+\Delta t}$ are the intensities of the solar radiation at time t and after the current time interval, respectively; and A_L is the surface area of the solar pond.

2.3. Computational method

Based on the single factor experiment, four factors were selected to investigate the effect of the structure of the solar pond on the crystallization of Li_2CO_3 and the interaction between them. Using the Box-Behnken response surface method to arrange the experiment, the parameters for the optimal construction of the solar pond and regression relationship for extracting lithium from it were obtained. Also, the strength of the two-by-two interaction between the factors was visualized on a 3D surface plot of the response surface, where ellipse indicates that the interaction was significant, and the circle indicates non-significant interactions. The highest point of the response surface and the center point of the minimum ellipse in the contour represent the extreme values within the range of the factors investigated by the response values. The flow field inside the solar pond was simulated using the CFD module of the COMSOL Multiphysics software. At the same time, the fluid heat transfer physical field in the heat transfer module was used. In this simulation, the interaction between the flow field and fluid heat transfer was considered. The fluid flow and heat transfer interface were coupled, and the non-isothermal flow physical field was added.

In the fluid heat transfer part, the heat balance equation was used to obtain the temperature distribution during the overall fluid heat transfer, which can be expressed by Eq. (4).

$$\begin{aligned} &\rho C_p \mathbf{u} \cdot \nabla T + \nabla \cdot \mathbf{q} = Q + Q_p + Q_{vd} \\ &\mathbf{q} = -k \nabla T \end{aligned} \tag{4}$$

where T is the temperature; C_p is the specific heat capacity at atmospheric pressure; $\mathbf{u}$ is the velocity vector brought in by the previous step; $\mathbf{q}$ is the heat flux; and Q , Q_p and Q_{vd} are three internal heat source terms.

This simulation needed to add a non-isothermal flow multi-physical field to couple the laminar flow and fluid heat transfer interface, which could more accurately simulate the flow and heat transfer behavior of the fluid under the

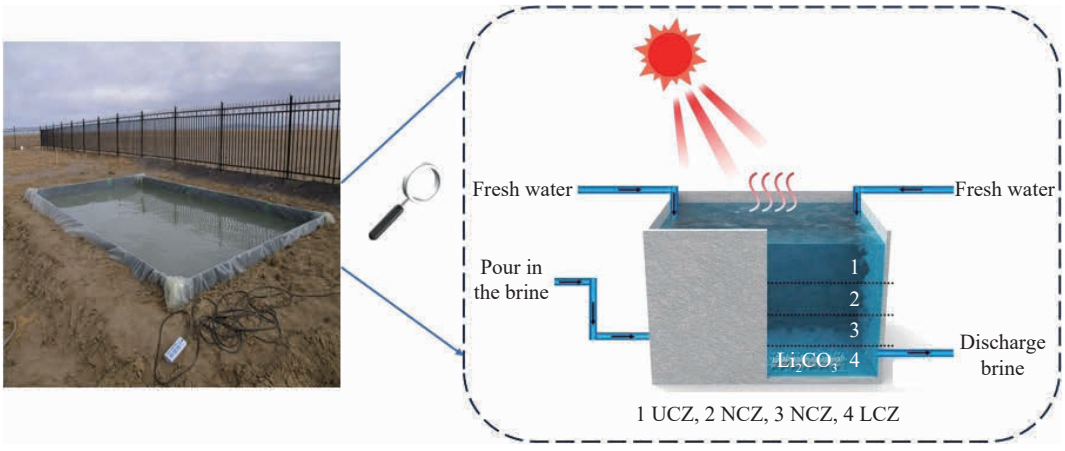

Fig. 1. Schematic diagram of the construction of extraction lithium solar pond.

temperature gradient. This flow field can be expressed by Eq. (5).

$$Q_{vd} = \tau : \nabla \mathbf{u} \tag{5}$$

where τ is the stress tensor, and **u** is the velocity vector.

Since the density of the gradient in the middle of the NCZ layer of the solar pond varies, the lower is high and the upper is low, so in the multi-physical field of non-isothermal flow, it is necessary to select the material property as the Boussinesq approximation, and the material density is specified as linear change, considering the buoyancy effect caused by temperature change as in Eq. (6).

$$\mu = \mu(p_{ref}, T_{ref}), Cp = Cp(T_{ref}), k = k(T_{ref}) \tag{6}$$

$$\mathbf{F_g} = \rho_{ref}(1 - \alpha_{p,0,ref})(T - T_{ref})\mathbf{g}$$

where μ is dynamic viscosity, p_{ref} is the reference pressure, T_{ref} is the reference temperature, F_g is buoyancy, ρ_{ref} is the reference density, α_{ref} is the coefficient of thermal expansion, and g is the acceleration due to gravity.

3. Results and discussion

3.1. UCZ thickness and icing

The UCZ water body is equivalent to the anti-interference layer of the solar pond, and its thickness and stability affect the heat collection in the entire solar pond. It can be seen from Fig. 2 that the temperature in the UCZ layer increased rapidly at the initial stage of operation. After 5 to 10 days, the temperature in each pond reached to about 25°C. The solar pond with a greater thickness of the UCZ layer warmed up more quickly after 10 days. However, the increase in temperature in the solar ponds with the UCZ thickness of 30–60cm was similar, reaching the highest value with a little difference. The final temperature in the solar ponds with different UCZ thickness values was 50–55°C after 40–50 days of operation. Where the thickness of the UCZ layer was greater than 60cm, the heating rate and final temperature were lower. This is because the energy collected by the solar pond was derived entirely from the solar radiation energy reaching the surface of the pond. In order to collect the maximum amount of energy or to maximize the available energy, it is necessary to allow as much solar radiation into the LCZ layer as possible. However, the solar radiation entering the LCZ layer is absorbed, reflected and scattered by the UCZ and NCZ layers. The larger the thickness of the UCZ and NCZ layers, the less the solar radiation entering the LCZ layer, the slower the temperature rise in the solar pond, and the lower the temperature that could be reached.

The UCZ layer in the solar pond gets frozen in winter, which increases the salinity beneath the ice. The transmissibility of ice affects the amount of solar radiation. The solar pond is a typical thermohaline double diffusion system. A change in heat leads to changes in concentration, temperature and pressure, which in turn changes the salt transport process and affects the precipitation of lithium carbonate. Through a comparative experiment with three frozen solar ponds having the same UCZ thickness, the solar ponds with a cleared icing layer, a retained icing layer, and a double-layer icing layer, and the radiometer was placed at the interface of the UCZ and the NCZ. The obtained monitoring results are shown in Fig. 3, where it can be noticed that the light intensity under ice was closely related to the thickness of the ice layer, and the light transmittance through the ice layer varied with the change in solar position and intensity of solar radiation. With an increase in the incident angle of sunlight and enhancement of solar irradiation, the transmittance through the ice layer to sunlight was getting better and better, and the maximum radiation transmittance through the single ice layer was 1.28 times of that through the double ice layer. With an increase in the thickness of the ice layer, the transmittance generally shows a downward trend. Therefore, the ice layer should be cleaned in time during winter to ensure the light transmittance through the UCZ layer.

3.2. Number of NCZ layers

For NCZ, 0–5 layers were set, each layer of 5 cm thickness. The obtained experimental results are shown in

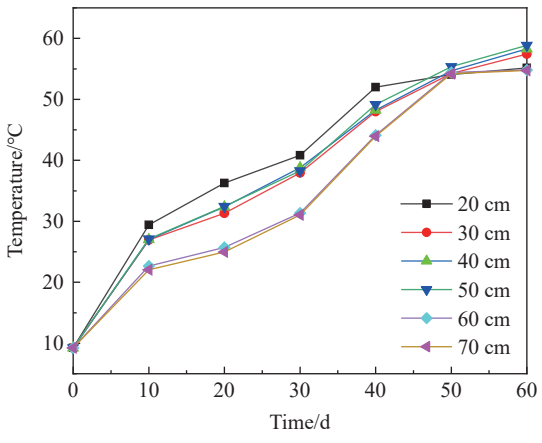

Fig. 2. Setting of LCZ temperature of UCZ with different thickness.

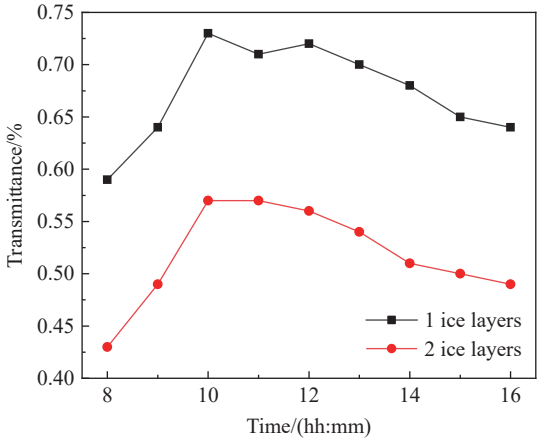

Fig. 3. Radiative transmittance through different ice layers.

Fig. 4. In the solar pond without NCZ, when the sun irradiation heated up the LCZ layer rapidly, a small amount of lithium carbonate precipitated, and the heat collected at night was lower than the heat dissipation, resulting to gradual cooling of the layer. Its thermal insulation effect was poor, temperature showed a periodic cycle, and the overall temperature was low, which could not be used for the purpose of precipitation of lithium carbonate. The temperature of the solar pond with 1 layer of NCZ was similar to that without NCZ, and the temperature increased faster but without any heat preservation.

The thermal efficiency of solar pond refers to its ability to convert solar radiation into energy, which is an important index to reflect the performance of the solar pond. Fig. 5 shows the thermal efficiency of the solar pond with different NCZ layers. Among the six solar ponds, the thermal efficiency of the solar pond without NCZ is 18.12%, while those of the solar ponds with 1–5 layers of NCZ were 18.69%, 18.84%, 18.97%, 15.94% and 15.12%, respectively. It implies that as the number of NCZ layers increases, the thermal efficiency of the solar pond first increases and then decreases.

In case of different numbers of NCZ layers, different numbers of reflection surfaces will be generated even for the same incident light intensity, thus reducing the transmission energy, reducing the radiation energy reaching the LCZ layer.

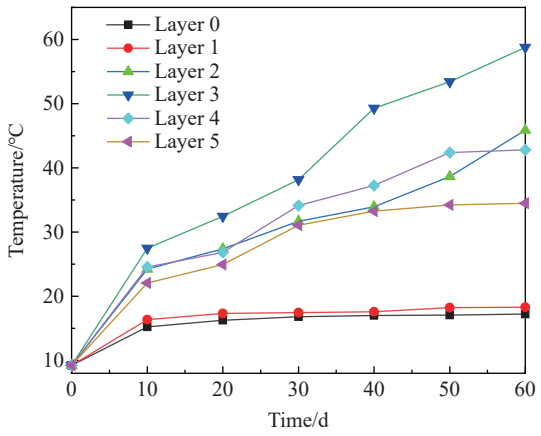

Fig. 4. Heating map of solar pod with different layers of NCZ.

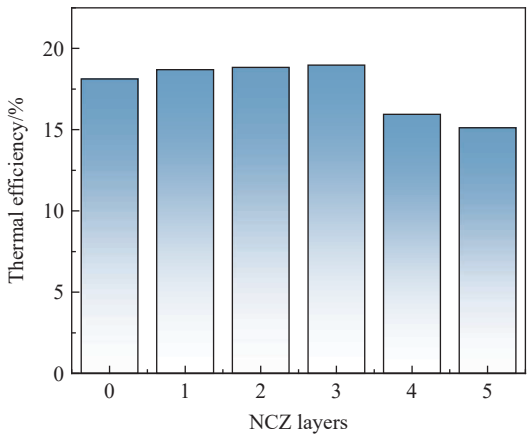

Fig. 5. Thermal efficiency of solar ponds with different NCZ layers.

Therefore, the solar pond with fewer NCZ layers will have more solar radiation energy reaching the LCZ layer, which will improve its heat collection performance. On the contrary, the solar pond with more NCZ layers has more reflection surfaces and more corresponding reflection energy consumption, resulting in lower radiation energy reaching the LCZ area and poor heat collection effect. Therefore, under the same radiation intensity, the solar pond with more NCZ layers absorbs less solar energy than the one with fewer NCZ layers in the same time period, resulting in low heat collection efficiency. However, another aspect related to the thermal efficiency of the solar pond is its heat storage performance. When the number of NCZ layers is high, the LCZ layer transfers heat upward through the solution will pass through each gradient layer in the NCZ layer, delaying the speed of upward energy transmission (the thermal conductivity of water is 0.654 $W/m^2 \cdot °C$ at 60 °C, and the thermal insulation effect of 1 m thick water layer is equivalent to more than 10 cm of asbestos), slowing down the dissipation of heat, making the solar pond with more NCZ layers have relatively high heat storage efficiency. Therefore, the thermal efficiency of a solar pond depends upon its both heat collection efficiency and heat storage efficiency. Increase in the number of NCZ layers will reduce the heat collection efficiency, but increase the heat storage efficiency. In the process of lithium extraction from the solar pond, it is necessary to use the construction characteristics of the NCZ layers. When the climatic temperature is low, only a fewer layers can be built for rapid heating. Once the temperature is increased, the number of NCZ layers can be increased for rapid heat collection and more heat storage, and also to improve the volume and rate of precipitation of lithium carbonate.

3.3. Effect of LCZ heating method on crystallization of Li2CO3

Fig. 6 shows the *c-t* curves of the pre-sun-concentrated brine injected directly into LCZ at 40°C, 50°C, 60°C and 70°C. The direct warming led to rapid increase in the initial supersaturation of lithium carbonate in brine. The sudden increase in supersaturation was sufficient to overcome the resistance of phase transition. Due to the formation and growth of new crystal nuclei, there was no obvious induction period in the *c-t* curve of brine. When the lithium carbonate crystal grew to a certain extent due to the sedimentation under gravity, the crystal nucleus in the solution decreased, width of the metastable zone became smaller, and the concentration curve became very smooth. From the crystallization characteristics of lithium carbonate, the precipitation could be preliminarily determined as the pre-sun-concentrated brine was directly injected into the LCZ layer. The formation of the crystal nucleus during the crystallization of the lithium carbonate, the saturated solution was mainly primary nucleation (heterogeneous nucleation), followed by the crystal growth attached to the crystal nucleus, and rapid precipitation of lithium carbonate.

Fig. 7 shows the crystallization of pre-sunning brine at a

controlled heating rate. During the heating process, the Li^+ concentration in the brine changed slowly for a certain period of time, followed by a period of rapid decline and finally flattening out. The induced period for controlled rate of crystallization was more pronounced, with the brine appearing to crystallize as it was warmed up to 30°C. The driving force for the crystalline precipitation process was the degree of supersaturation. The precipitation of lithium carbonate with slow heating of brine is a gradual staged process. As the temperature rises, the supersaturation gradually increases, and the solution enters the unstable region from the metastable region. When a certain degree of supersaturation is reached, lithium carbonate crystals begin to precipitate, as shown in the study of the slow crystallization process of the insoluble salt calcium carbonate. When the brine continues to rise to a certain temperature, the supersaturation reaches a critical value, and the crystallization mechanism becomes heterogeneous nucleation. Subsequently, the crystallized lithium carbonate crystal grows in the solution and settles down under the action of gravity after reaching a certain particle size. At this moment, as the solution continues to heat up, it can maintain a supersaturation, but it would be much smaller than the critical supersaturation. The sedimentation process of lithium carbonate crystal and the shear force

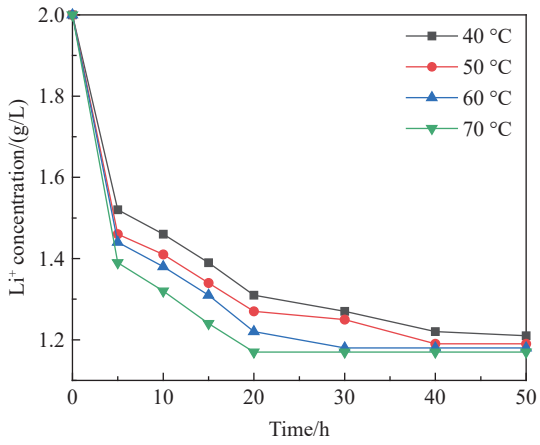

Fig. 6. *c-t* curves of pre-sunning brine into LCZ at 40°C, 50°C, 60°C and 70°C.

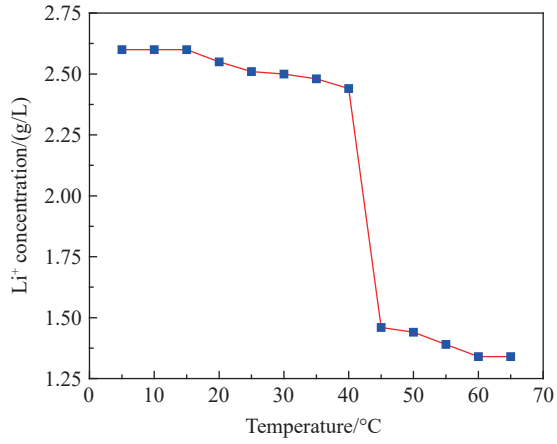

Fig. 7. *c-t* curve of lithium carbonate in desorption solution and bath brine during controlled temperature rise.

generated by the solution form a part of small crystal nuclei, and there will a secondary nucleation. Using the solar pond technology for lithium extraction, the induction period of the controlled temperature rise can be increased and the efficiency of lithium extraction can be decreased. In the production application, the heating time of the solar pond can be prolonged, the initial temperature can be increased, and the efficiency of lithium extraction can be improved.

3.4. Effect of LCZ heating method on crystallization of Li_2CO_3

The isothermal evaporation experiment on salt crystallization revealed that natron ($Na_2CO_3 \cdot 10H_2O$) is an important product of brine evaporation. A large amount of natron is accumulated in the development of liquid lithium mine in the Zabuye salt lake. However, the transportation of that natron is not only economically expensive but it will also create various environmental problems. According to the common ion effect $2Li^+ + CO_3^{2-} \rightleftharpoons Li_2CO_3$, the addition of CO_3^{2-} in the solar pond brine may promote the reaction to move to the right, causing more precipitation of Li^+ in the brine in the form of Li_2CO_3. Therefore, through the common ion effect experiment, the natron can be continuously circulated in the salt lake to turn the waste into the treasure of the natron. The direct heating crystallization experiment at 50°C was carried out with the sunning pond brine. Three concentrations of Li^+ (1.5 g/L, 2.5 g/L and 2.5 g/L) and six concentrations of CO_3^{2-} (15 g/L, 20 g/L, 25 g/L, 30 g/L, 35 g/L and 40 g/L) were set, 50 mL of each solution was taken and 3 g of natron was added. The dynamic receiver was used for sampling and analysis. The obtained experimental results are shown in Fig. 8.

It was found that Li^+ of concentration of 1.5 g/L solar pond brine still had a part of natron undissolved, and the change in Li^+ concentration after adding natron was not obvious. The precipitation process of lithium carbonate is related to the concentration of CO_3^{2-} in the brine of the solar pond. When the concentration of CO_3^{2-} was less than 25 g/L, the addition of natron could accelerate the precipitation of lithium carbonate. After adding natron to brine with Li^+ concentration of 2.0 g/L, the precipitation amount of lithium carbonate increased by 0.13 g/L. The higher the concentration of Li^+, the faster is the precipitation of lithium carbonate after the addition of natron. When the concentrations of CO_3^{2-} in the brine were 35 g/L and 40 g/L, lithium carbonate was basically no longer precipitated in the brine regardless of the concentration of Li^+ in the brine. During the lithium extraction process in the solar pond, the concentration of Li+ in the brine used for brine irrigation needs to be greater than 2.0 g/L, while the concentration of CO_3^{2-} should be less than 30 g/L. In this concentration range, the addition of natron will significantly enhance the crystallization efficiency of lithium carbonate and the amount of precipitation.

3.5. Optimized route

The response surface method is an optimization method that integrates experimental design and mathematical

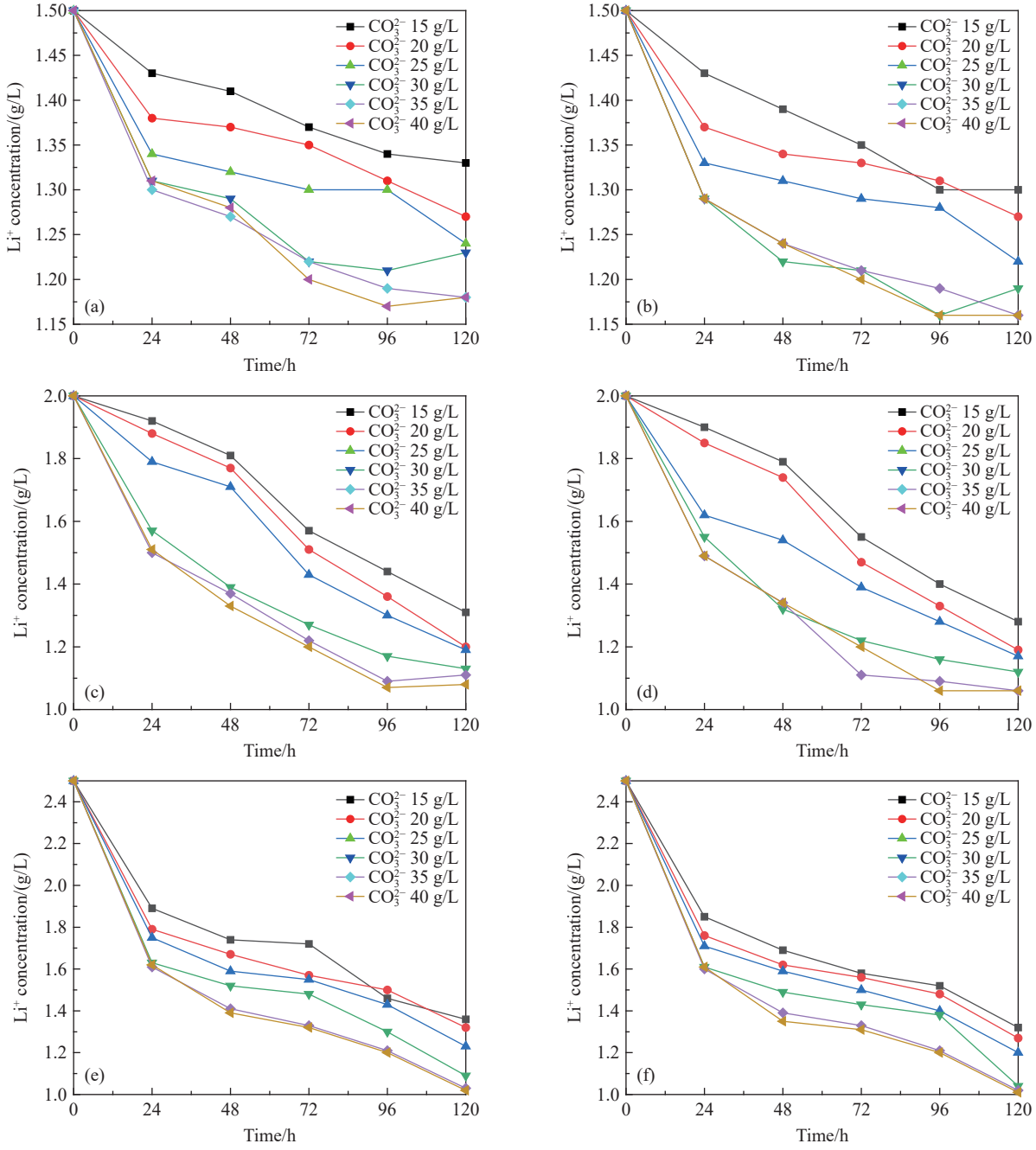

Fig. 8. *c-t* curves of constant temperature rise (a,c,e) and direct temperature rise (b,d,f) to 50°C.

modeling. Through experiments on representative local points, a regression equation is used to fit the functional relationship between the factors and results in the global range, and the importance of each response value is integrated to give the optimal level value of each factor. Because of the advantages of high accuracy and good predictive performance, it is widely used in many fields. The application of this study is based on the principles of the Box-Behnken experimental design. In order to optimize the Li^+ concentration at equilibrium four factors were determined under different conditions. The determined four factors include the thickness of UCZ, temperature of direct temperature rise, concentration of CO_3^{2-}, and concentration of the added natron. The Li^+ concentration at equilibrium was used as the response value (Y) to optimize the crystallization process using the method of response surface experiments and Box-Behnken experimental design as shown in Table 1.

According to the Box-Behnken combination design of 4 factors and 3 levels of response surface test, 25 experiments were carried out according to the process parameters listed in Table 2.

$$Y=1.13+0.052^{*}\ A-0.11^{*}\ B-0.066^{*}\ C+0.053^{*}\ D+0.025^{*}\ AB-0.035^{*}\ AC+0.045^{*}\ AD-0.02^{*}\ BC+0.078^{*}\ BD-0.017^{*}\ CD+0.049^{*}\ A^2+0.17^{*}\ B^2+0.065^{*}\ C^2+0.074^{*}\ D^2$$

As can be seen from Table 3, the difference between the models was highly significant ($P<0.001$), and the coefficient of determination R^2 was 0.9736, indicating that the fitting of the model was excellent and it could fit the test results more

intuitively. The misfit term was not significant ($P > 0.05$), indicating that the model error was small. The corrected determination coefficient R^2_{Adj} was 0.9473, indicating that the correlation and interpretation of the model were good. This model can be used for theoretical analysis and prediction.

The value of index F was important for evaluating the influence of each variable on the response value. The larger the F value, the higher was the contribution of the relevant model components to the response. When the significance test probability was $P<0.05$, it revealed that the variable had a significant effect on the response value, which was statistically significant. Analyzing the effects of each factor on the Li^+ concentration at equilibrium, it was found that the effects of the primary terms LCZ temperature, UCZ thickness, CO_3^{2-} concentration, and addition of natronite had highly significant on the Li^+ concentration at equilibrium ($P<0.01$). The order of effects of these four factors on the Li^+ concentration at equilibrium was B>C>D>A, i.e., LCZ temperature>CO_3^{2-} concentration>added natronite concentration>UCZ thickness. The effects of the secondary terms A2, B2, C2, and D2 on the concentration of Li^+ at equilibrium were highly significant ($P<0.01$), which indicated that these three factors had nonlinear effects on the concentration of Li^+ at equilibrium. The interaction term BD had a highly significant effect on the Li^+ concentration at equilibrium ($P<0.01$), and AC and AD had significant effects on the Li^+ concentration at equilibrium ($P<0.05$).

The AB interaction is shown in Fig. 9. On the AB

Table 1. Levels and codes of Box-Behnken.

Factor	Level		
	−1	0	1
A-UCZ Thickness (cm)	50	55	60
B-Temperature (°C)	50	55	60
C-CO_3^{2-} Concentration (g/L)	25	30	35
D-Natronite (g/L)	6	7	8

Table 2. Experimental design and results of Li^+ concentration in response surface optimization equilibrium.

Number	A (cm)	B (°C)	C (g/L)	D (g/L)	Y
1	50	50	30	7	1.42
2	60	50	30	7	1.51
3	50	60	30	7	1.15
4	60	60	30	7	1.34
5	55	55	25	6	1.28
6	55	55	35	6	1.14
7	55	55	25	8	1.44
8	55	55	35	8	1.23
9	50	55	30	6	1.19
10	60	55	30	6	1.20
11	50	55	30	8	1.21
12	60	55	30	8	1.40
13	55	50	25	7	1.50
14	55	60	25	7	1.36
15	55	50	35	7	1.41
16	55	60	35	7	1.19
17	50	55	25	7	1.23
18	60	55	25	7	1.37
19	50	55	35	7	1.21
20	60	55	35	7	1.21
21	55	50	30	6	1.56
22	55	60	30	6	1.13
23	55	50	30	8	1.49
24	55	60	30	8	1.37
25	55	55	30	7	1.12

Table 3. Analysis of variance and results with quadratic model of Li^+ concentration.

Source	Sum of squares	Degree of freedom	Mean square	F value	P value	Significance
Model	0.52	14	0.037	36.94	<0.0001	**
A- UCZ Thickness (cm)	0.032	1	0.032	31.74	<0.0001	**
B- Temperature (°C)	0.15	1	0.15	150.50	<0.0001	**
C-CO_3^{2-} Concentration (g/L)	0.052	1	0.052	51.54	<0.0001	**
D- Natronite (g/L)	0.034	1	0.034	33.82	<0.0001	**
AB	2.500E-003	1	2.500E-003	2.48	0.1378	
AC	4.900E-003	1	4.900E-003	4.86	0.0448	*
AD	8.100E-003	1	8.100E-003	8.03	0.0133	*
BC	1.600E-003	1	1.600E-003	1.59	0.2286	
BD	0.024	1	0.024	23.81	0.0002	**
CD	1.225E-003	1	1.225E-003	1.21	0.2891	
A^2	0.015	1	0.015	15.33	0.0016	**
B^2	0.19	1	0.19	191.45	<0.0001	**
C^2	0.027	1	0.027	27.23	0.0001	**
D^2	0.035	1	0.035	35.04	<0.0001	**
Residual	0.014	14	1.009E-003			
Lack of fit	0.012	10	1.221E-003	2.54	0.1909	ns
Pure error	1.920E-003	4	4.800E-004			
Cor total	0.54	28				

R^2=0.9736 R^2_{Adj}=0.9473 R^2_{Pre} =0.8632

Note: $P<0.01$ is extremely significant, indicated by **; $P<0.05$ is significant, indicated by *; $P>0.05$ is not significant, indicated by ns.

interaction surface, the Li^+ concentration at equilibrium decreased slowly as the thickness of the freshwater layer increased. The Li^+ concentration at equilibrium first decreased and then increased as the direct warming increased the process. Considering only the interaction between the two, it was found that the Li^+ concentration at equilibrium was smaller (i.e., more Li_2CO_3 precipitated) when the direct heating was around 54–60°C and the freshwater layer thickness was about 50–56 cm.

The *AC* interaction is shown in Fig.10. On the AC interaction surface, the Li^+ concentration at equilibrium first showed a gentle trend and then an increasing trend. When the UCZ thickness was low, the carbonate concentration increased, and the concentration of Li^+ decreased first and then increased. When the UCZ thickness and CO_3^{2-}concentration were large, with increase in the CO_3^{2-} concentration, the Y value first decreased and then flattened, indicating that there was a significant interaction between the UCZ thickness and CO_3^{2-} concentration. Considering only the two interactions, it could be obtained that the Li^+ concentration at equilibrium was smaller when the CO_3^{2-} concentration was around 27–35 g/L and UCZ thickness was around 50–56 cm.

The *AD* interaction is shown in Fig. 11. On the *AD* interaction surface, when the addition of natron was less, the *Y* value first increased and then decreased with increasing UCZ thickness. When the addition of natron was more, with increasing UCZ thickness, the *Y* value first showed a gentle tendency and then increased. When the thickness of UCZ was small, with increasing natron, the *Y* value first decreased and then increased. When the thickness of UCZ was high, with increasing natron, the *Y* value was first gentle and then increased. This indicated that there was a significant interaction between the thickness of UCZ and concentration of natron. Considering only the interaction between the two, it was learnt that the *Y* value was smaller when the addition of added vesicant was around 6–7.5 g/L and the thickness of UCZ was around 50–58 cm.

The *BC* interaction is shown in Fig. 12. On the *BC* interaction surface, with increasing LCZ temperature, the *Y* value first decreased and then increased, and with increasing CO_3^{2-} concentration, the same first decreased and then flattened. Considering only the two interactions, it could be obtained that the *Y* value was smaller when the LCZ

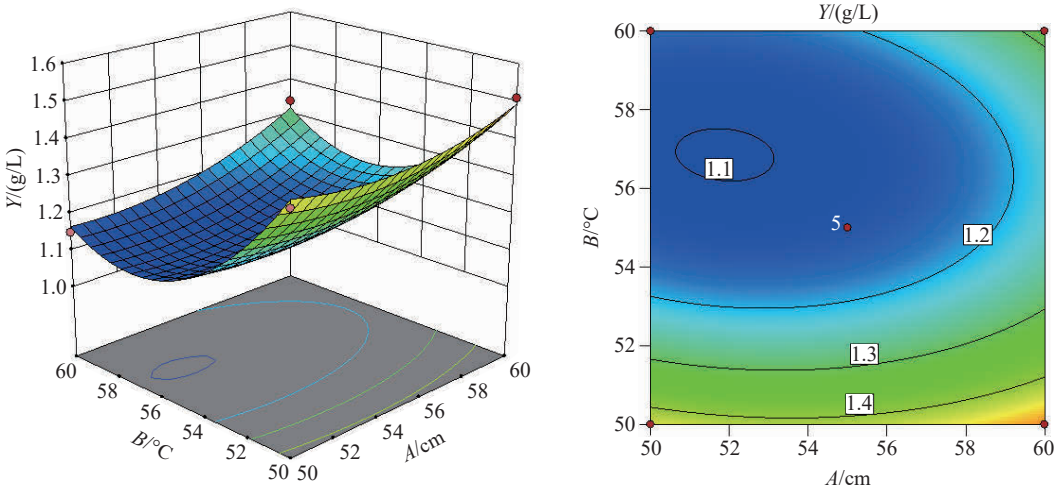

Fig. 9. Effect of *AB* interaction on *Y*.

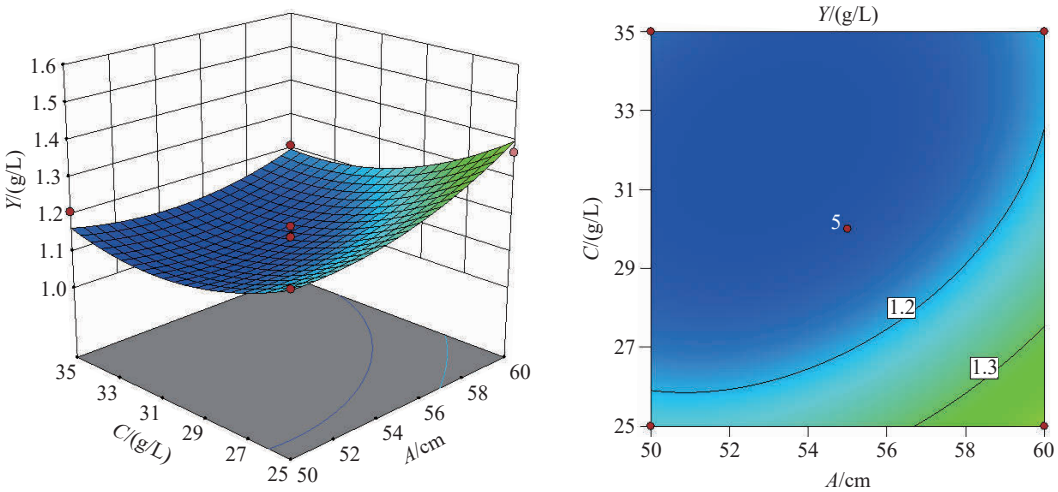

Fig. 10. Effect of *AC* interaction on *Y*.

temperature was around 54–60°C and CO_3^{2-} concentration was around 29–35 g/L.

The *BD* interaction is shown in Fig. 13. On the *BD* interaction surface, when the concentration of natron was low, *Y* decreased first and then increased with increasing LCZ temperature. When the concentration of natron was high, *Y* decreased first and then increased with increasing LCZ temperature. When the LCZ temperature was low, *Y* decreased first and then increased with increasing natron concentration. When the LCZ temperature was high, *Y* increased with increasing natron concentration, indicating that there was a significant interaction between the LCZ temperature and natron concentration. Considering only the interaction between the two, it was learnt that *Y* was smaller when the LCZ temperature was around 54–60°C and the concentration of added natron was around 6–7 g/L.

The *CD* interaction is shown in Fig. 14. On the *CD* interaction surface, with increasing concentration of natron, *Y* decreased first and then increased. With increasing CO_3^{2-} concentration, *Y* decreased first and then leveled off. Considering only the interaction between the two, it could be obtained that *Y* was smaller when the concentration of added natron was around 6–7 g/L and concentration of CO_3^{2-} was around 29–35 g/L.

Taking the maximization of the Li_2CO_3 precipitation (i.e., the minimization of the Li^+ concentration at equilibrium) as the optimization objective, the experiment was optimized by the Design-Expert 10.0.3 software. The predicted Li^+ concentration at equilibrium was 1.07 g/L. The predicted values of the four factors, namely the UCZ thickness, LCZ direct heating temperature, CO_3^{2-} concentration, and added natron concentration, where 53.63 cm, 57.39°C, 32.21 g/L, and 6.52 g/L, respectively.

3.6. Analysis of effect of lithium extraction after optimization

Experiments were conducted to verify the effect of optimization. For the convenience of operation, the values of condition parameters, namely the UCZ thickness, LCZ direct heating temperature, carbonate concentration, and addition of natron concentration, were set to be 54 cm, 57°C, 32 g/L, and 6.5 g/L, respectively. The experiments were repeated three times under the condition. The average Li^+ concentration at equilibrium was measured to be 1.05 g/L, which was within 5% deviation from the model prediction value of 1.07 g/L,

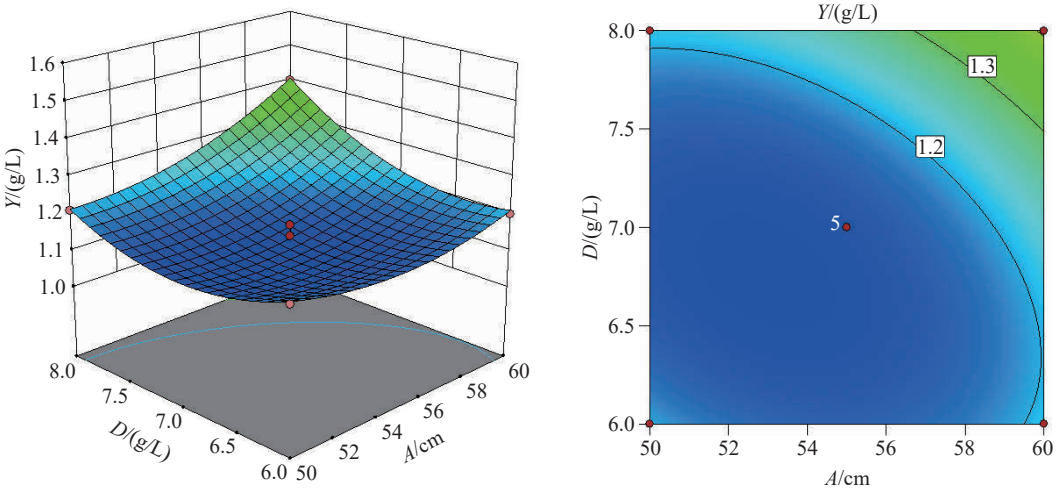

Fig. 11. Effect of *AD* interaction on *Y*.

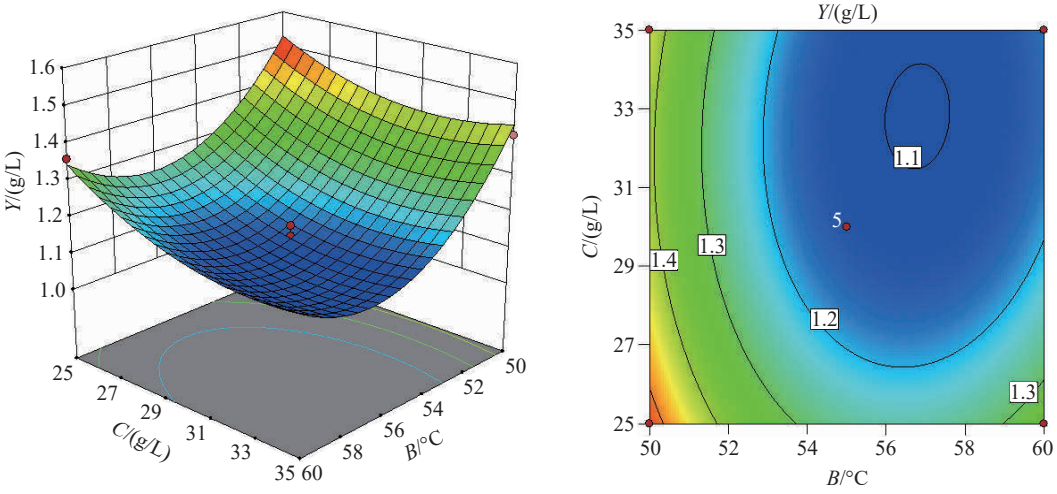

Fig. 12. Effect of *BC* interaction on *Y*.

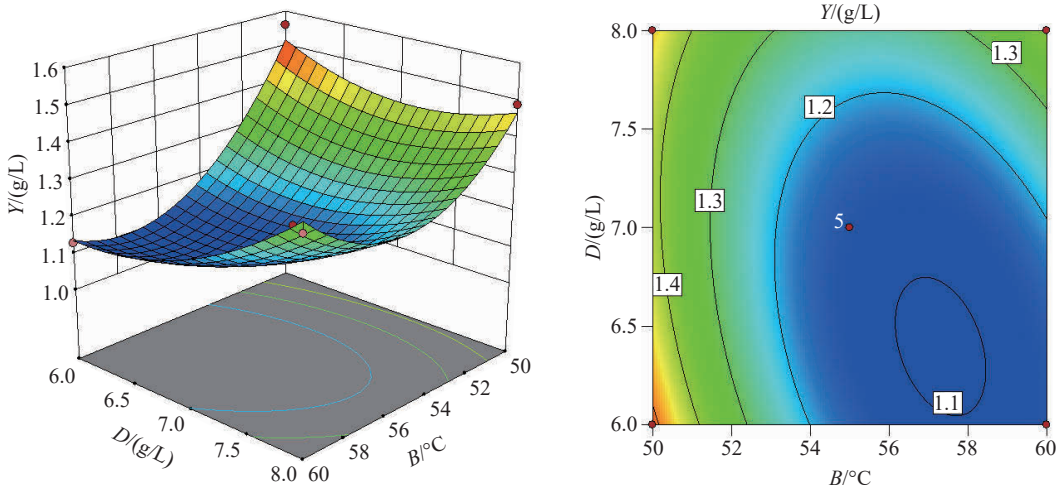

Fig. 13. Effect of *BD* interaction on *Y*.

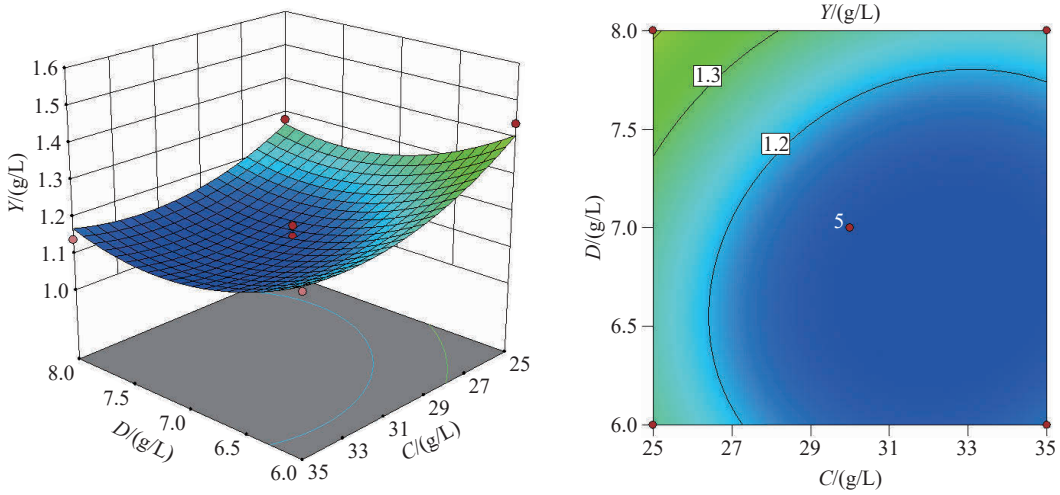

Fig. 14. Effect of *CD* interaction on *Y*.

indicating that the optimized process parameters were reliable.

After pretreatment by the Zabuye process, concentrated brine was injected into LCZ. Then, the solar pond was constructed according to the optimized route, and compared it with the original solar pond. After optimization, Li_2CO_3 in the solar pond could reach the precipitation equilibrium within 60 hours, which increased the crystallization rate of lithium carbonate by 33.33% compared to the initial solar pond process (Fig. 15). Also, the extracted amount of Li_2CO_3 was increased by 7.34%. Both lithium extraction rate and production were improved after optimization.

As can be seen from the diagrams of temperature field distribution before and after optimization of the lithium extraction solar pond in Zabuye salt lake (Fig. 16), the temperature field was more widely distributed and the temperature was higher after optimization. For lithium extraction from solar pond, temperature has the greatest influence on Li_2CO_3 precipitation. In the above study, the initial supersaturation of Li_2CO_3 in brine increased rapidly with direct heating, and a sudden increase in supersaturation was enough to overcome the resistance of the phase transition.

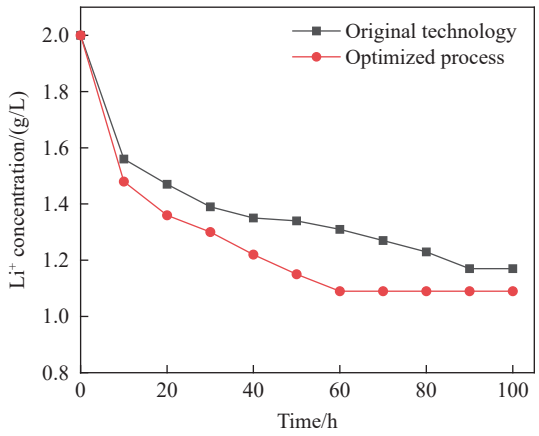

Fig. 15. Comparison of crystallization before and after optimization of lithium extraction solar pond process in Zabuye salt lake.

The supersaturation increased at the highest rate, which was more conducive to the nucleation and growth of crystals. Therefore, after optimization, the precipitation balance of Li_2CO_3 in the solar pond was faster and more Li_2CO_3 was produced.

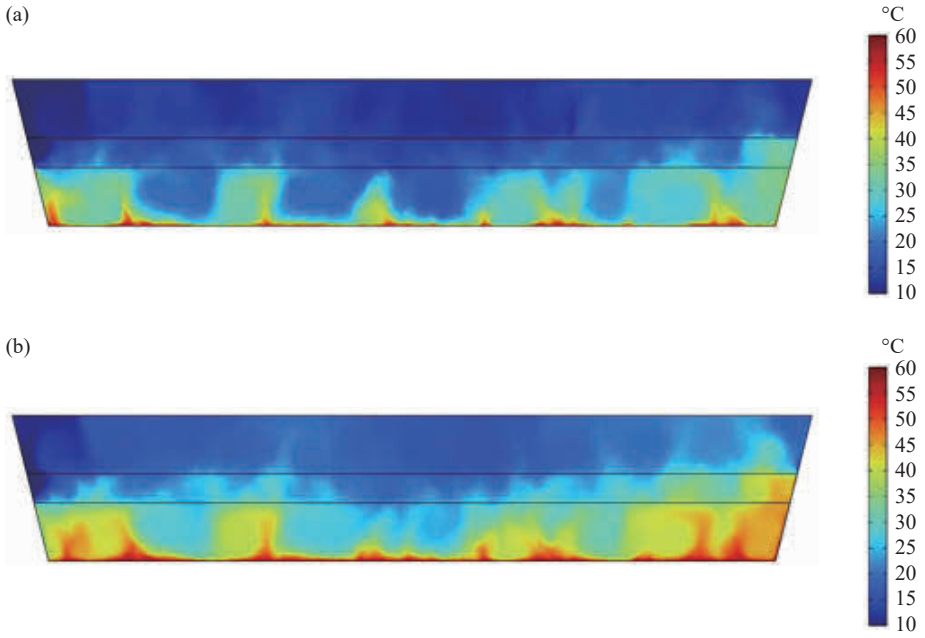

Fig. 16. Distribution of temperature field: a–before optimization and; b–after optimization.

4. Conclusion

In this work, the process of lithium extraction from solar pond in the Zabuye salt lake was optimized by a laboratory-base experimental setup combined with a simulation model. The optimization route was determined by the Design-Expert 10.0.3 software, and the Li^+ concentration at the predicted equilibrium was found to be 1.07 g/L. The predicted values of four factors, namely UCZ thickness, LCZ direct heating temperature, CO_3^{2-} concentration, and addition of natron, were found to be 53.63 cm, 57.39°C, 32.21 g/L, and 6.52 g/L, respectively. The experiment was repeated three times according to the optimized process. The average concentration of Li^+ at equilibrium was found to be 1.05 g/L, which was within 5% deviation from the predicted value of 1.07 g/L, indicating that the process parameters optimized by the model were reliable. After optimization, Li_2CO_3 in the solar pond could reach the precipitation equilibrium within 60 hours, which increased the crystallization rate of lithium carbonate by 33.33% compared to the initial solar pond process and its extracted amount was increased by 7.34%. Both lithium extraction rate and production were improved after optimization.

CRediT authorship contribution statement

Tao Ding, Qian Wu, Jiang-jiang Yu, Ling-zhong Bu, Yun-sheng Wang, En-yuan Xing and Yu-bin Li prepared the manuscript. Tao Ding drew all the figures. Zhen Nie and Mian-ping Zheng supervised the findings of this work. All authors discussed the results and contributed to the final manuscript.

Declarations of interest

The authors declare no conflicts of interest.

Acknowledgement

The author thanks the reviewers and editors who participated in the manuscript review. This study was supported by the National Natural Science Foundation of China (U20A20148) and the Major Science and Technology Projects of the Xizang (Tibet) Autonomous Region (XZ202201ZD0004G and XZ202201ZD0004G01).

References

Abdullah AA, Fallatah HM, Lindsay KA, Oreijah MM. 2017. Measurements of the performance of the experimental salt-gradient solar pond at Makkah one year after commissioning. Solar energy, 150, 212–219. doi: 10.1016/j.solener.2017.04.040.

Alcaraz A, Montalà M, Cortina JL, Akbarzadeh A, Aladjem C, Farran A, Valderrama C. 2018. Design construction and operation of the first industrial salinity-gradient solar pond in Europe: An efficiency analysis perspective. Solar energy, 164, 316–326. doi: 10.1016/j.solener.2018.02.053.

Alcaraz A, Montala M, Valderrama C, Cortina JL, Akbarzadeh A, Farran A. 2018. Increasing the storage capacity of a solar pond by using solar thermal collectors: Heat extraction and heat supply processes using in-pond heat exchangers. Solar Energy, 171, 112–121. doi: 10.1016/j.solener.2018.06.061.

Bisht S, Dhindsa GS, Sehgal SS. 2020. Augmentation of diurnal and nocturnal distillate of solar still having wicks in the basin and integrated with solar pond. Materials Today Proceedings, 33(3), 1615–1619. doi: 10.1016/j.matpr.2020.05.732.

Bozkurt I, Deniz S, Karakilcik M, Dincer I. 2015. Performance assessment of a magnesium chloride saturated solar pond. Renewable Energy, 78, 35–41. doi: 10.1016/j.renene.2014.12.060.

Ding T, Zheng MP, Nie Z, Ma LC, Ye CY, Wu Q, Zhao YY, Yang DH, Wang K. 2022. Impact of regional climate change on the development of lithium resources in Zabuye Salt Lake, Tibet. Frontiers in Earth Science, 10, 865158. doi: 10.3389/feart.2022.865158.

Ding T, Zheng MP, Peng SP, Lin YH, Zhang XF, Li MM. 2023. Lithium extraction from salt lakes with different hydrochemical types in the Tibet Plateau. Geoscience Frontiers, 14(1), 101485. doi: 10.1016/j.gsf.2022.101485.

Ding T, Zheng MP, Peng SP, Nie Z, Lin YH, Wu Q. 2022. Recovery of lithium ions from salt lakes using nanofibers containing zeolite carriers. Frontiers in Energy Research, 10, 895681. doi: 10.3389/fenrg.2022.895681.

Kaushika ND. 1984. Solar Pond: A review. Energy Conversation and Management. 353–376. doi: 10.1016/0196-8904(84)90016-5.

Li N, Wang Q, Liu JW. 2021 Experimental study on effect of nanoparticles on thermal performance of salt gradient solar pond. Thermal Science and Technology, 2021, 20(2), 122–127. (in Chinese). doi. 10.13738/j.issn.1671-8097.020106

Nie Z, Bu LZ, Zheng MP, Huang WN. 2011. Experimental study of natural brine solar ponds in Tibet. Solar Energy, 85(7), 1537–1542. doi: 10.1016/j.solener.2011.04.011.

Nie Z, Wu Q, Ding T, Bu LZ. 2022. Research progress on industrialization technology of lithium extraction from salt lake brine in China. Inorganic Chemicals Industry, 54(10), 1–12.

Rioyo J, Tuset S, Grau R. 2022. Lithium extraction from spodumene by the traditional sulfuric acid process: A review. Mineral Processing and Extractive Metallurgy Review, 43(1), 97–106. doi: 10.1080/08827508.2020.1798234.

Sayer AH, Al-Hussaini H, Campbell AN. 2018. New comprehensive investigation on the feasibility of the gel solar pond, and a comparison with the salinity gradient solar pond. Applied Thermal Engineering, 130, 672–683. doi: 10.1016/j.applthermaleng.2017.11.056.

Tahat MA, Kodah ZH, Probert SD, Tahaineh AI. 2000. Performance of a portable mini solar-pond. Applied energy, 66(4), 299–310. doi: 10.1016/S0306-2619(00)00021-0.

Tang LJ, Zheng MP, Liu JH. 2009. Crystallization experiment of carbonate salt lake brine in simulated solar pool. Acta Geologica Sinica, 30(2), 249–255(in Chinese).

Wang J, Wang L, Xu H, Sheng L, He XM. 2024. Perception of fundamental science to boost lithium metal anodes toward practical application. Green Energy & Environment, 9(3), 454–472. doi: 10.1016/j.gee.2023.02.008.

Wu Q, Yu JJ, Bu LZ, Nie Z, Wang Y, Renchen N, He T, Zhang K, Zhang JT, He ZK. 2022. The application of an enhanced salinity-gradient solar pond with nucleation matrix in lithium extraction from Zabuye salt lake in Tibet. Solar Energy, 244, 104–114. doi: 10.1016/j.solener.2022.08.031.

Yu JJ, Zheng MP, Tang LJ. 2013. Comparison of lithium extraction from carbonate brine by laboratory simulation and solar pond. Advances in Chemical Industry, 32(6), 1248–1252(in Chinese).

Zheng MP, Xing EY, Zhang XF, Li MM, Che D, Bu LZ, Han JH, Ye CY. 2023. Classification and mineralization of global lithium deposits and lithium extraction technologies for exogenetic lithium deposits. China Geology, 6(4), 547–566. doi: 10.31035/cg2023061.